energies

MDPI

Article

A Mathematical Model for Home Appliances in a DC Home Nanogrid

Miguel Cordova-Fajardo [1,2,*,†] and Eduardo S. Tututi [2,†]

[1] Departamento de Ciencias Básicas, Instituto Tecnológico de Lázaro Cárdenas, Lázaro Cárdenas CP 60950, Michoacan, Mexico
[2] Facultad de Ciencias Físico Matemáticas, Universidad Michoacana de San Nicolas de Hidalgo, Morelia CP 58060, Michoacan, Mexico
* Correspondence: mangel.cordova@lcardenas.tecnm.mx
† These authors contributed equally to this work.

Abstract: A mathematical model for nonlinear loads, that contains, in its design, a switching power supply is presented. The model was tested in home appliances operating in a Direct Current Home Nanogrid (DCHN). Compact Fluorescent Lamps (CFLs) and LED lamps were used as nonlinear loads to study, through the model, the experimental results in the profile of ripple in voltage and current of the lamps. The profile of ripples, due to the home appliances, could be explained by the model, even in the simultaneous operation of two loads. Additionally, the effect of decreasing the ripple amplitude when an induction stove in standby mode was incorporated with the DCHN was analyzed.

Keywords: DC nanogrid; standby consumption; mathematical model; nonlinear loads; DC home appliances; distortion harmonic

check for updates

Citation: Cordova-Fajardo, M.; Tututi, E.S. A Mathematical Model for Home Appliances in a DC Home Nanogrid. *Energies* **2023**, *16*, 2957. https://doi.org/10.3390/en16072957

Academic Editor: Abu-Siada Ahmed

Received: 10 February 2023
Revised: 4 March 2023
Accepted: 15 March 2023
Published: 23 March 2023

Copyright: © 2023 by the authors. Licensee MDPI, Basel, Switzerland. This article is an open access article distributed under the terms and conditions of the Creative Commons Attribution (CC BY) license (https://creativecommons.org/licenses/by/4.0/).

1. Introduction

It is well known that nanogrids are the basic elements of more complex systems, such as microgrids or power systems, which are important to obtain real electric distributed systems. Currently, the importance of a home nanogrid arises from its facility to incorporate electric energy generation systems by means of Renewable Energy Sources (RES), to reduce the energy conversion stages, and to avoid synchronization problems, among others [1]. In the same way, incorporating an energy storage sector into a home nanogrid is very important in diminishing dependence on the network energy. This is crucial in rural areas, where access to the grid is limited [2–4]. The benefits that a DCHN presents are, among others, performance, simplicity of control and efficiency. The usage of DCHN has been rather poor, due to the absence of DC home appliances and the heavy presence of AC home appliances in the local market, many of which can also operate with DC voltage [3]. The common uses of appliances in a DCHN are, for example, cooking food, lighting, refrigeration or communication [5]. It is well known that CFL and LED lamps, and other home appliances, which we refer to as loads, are associated with the voltage and current distortion in AC systems [6,7]. The noise emission and pollution into the grid is related to the operation of high efficiency appliances in the nanogrid, which are emitted by their switching power supplies (SPSs) [8].

The resulting electrical behavior of these appliances is nonlinear and much effort has been made to understand and model them. There exist a lot of studies in the literature on models that use predefined blocks in labview or mathlab/symulink, which are based on knowledge of their internal components [9–14]. However, this knowledge is not necessary, as shown in [15], but, to complement simulation, measurements of some parameters in the model are required. There are many studies in the literature focused on how to diminish the distortion waveform, also called harmonics, produced by nonlinear loads in AC systems [16,17]. Similarly, in DC systems the harmonics are present as voltage and current

ripples. The development of Electromagnetic Interference Filter (EMI) provides a solution typical to AC systems [5,18,19] to diminish the intensity of harmonics. Nevertheless, the used filters consume energy, even in the state denominated as standby mode, which occurs when the home appliance in question spends energy without doing any real work.

On the other hand, in the case of the DCHN, little attention has been paid to the behavior of appliances and their modeling. Instead of studying the components and effects of the SPS, as part of an analysis of a DCHN, we are interested in comprehending the behavior of the voltage and current in the system. These are altered by the harmonics produced by the SPS in the appliances or other electric devices. A model, highlighting the behavior of nonlinear loads, regardless of the number, or kind, of appliances connected to the grid, could be useful in the design of more efficient energy storage systems, monitoring systems or wiring in the DCHN. In this paper, we propose a simple model for nonlinear loads, based upon the switching mode of an SPS. This model is quite general, and, as matter of fact, could be applicable to describe the nonlinear resistance behavior of any electric device containing, as a part of its design, an SPS sector. Nevertheless, in this paper, we only focus on discussing the application of the model in appliances in a DCHN and its simultaneous operation. The advantage of the model proposed consists in avoiding the use of Fourier series and it allows, in a rather simple way, the analysis of the corresponding circuit. Differing from other proposed models, in this proposal knowledge of the internal components of the device under consideration is not required.

An outline of this paper is as follows. In Section 2 we present the mathematical model for the nonlinear load. The mathematical model takes different theoretical values in Section 3 . In Section 4 the results of the experimental measurements are presented. In Section 5 we discuss the experimental data and compare the data with the numerical simulations. Finally, in Section 6 the conclusions are provided.

2. Mathematical Model

A general model for nonlinear loads operating on DC, where the internal components are, in principle, unknown is presented in this section. Although the motivation for constructing the model was based on home appliances in a DCHN, the possible applicability of the model is wide, since it is elaborated on basic principles and the assumption that the device in question has an SPS in its inner part. Let us first recall that nonlinear behavior is commonly described by resorting to continuous periodical functions, which allow the experimental data to be explained. For example, in the design of a DCHN, it is crucial to identify and characterize each component in the different sectors of the system. In the energy storage sector, a simple model for the batteries is established by the function $V_{Bat}(t) = V_d$ where V_d is a constant value. In the loads sector, it is usual to model the loads as linear, given by simple resistances, such as $R(t) = R_0$, and R_0 being a constant. The home appliances that are used in a DCHN are of high efficiency and employ SPS with low energy consumption. As was previously mentioned, these appliances have nonlinear behavior and must be considered as nonlinear loads. Thus, the appliances cannot be represented simply by a constant function R_0, and it is necessary for the model to contain and reproduce the electrical parameters of the appliance in the DCHN. This can be carried out through a mathematical description of nonlinear loads in a simple equivalent circuit.

For example, the AC voltage supplies are described by the function $V(t) = V_m \sin(\omega t)$ where V_m is the amplitude of the voltage and ω is the frequency. This simple model is used to determine other parameters, such as the impedance Z, without the previous knowledge of the AC generator engine.

The buck and booster converter are used in appliances. The effect on energy consumption of these converters is minimal. However, due to switching, they emit noise into the system. A buck converter, that includes an EMI filter, is represented in the circuit of Figure 1. The mode of operation of this circuit is as follows. At time, T_{OFF}, the circuit is opened and the EMI filter components are fed, which are directly connected to the A and B

nodes. At time T_{ON} (see Figure 2) the transistor feeds the LCR circuit, which maintains a constant voltage V_0 at R_E.

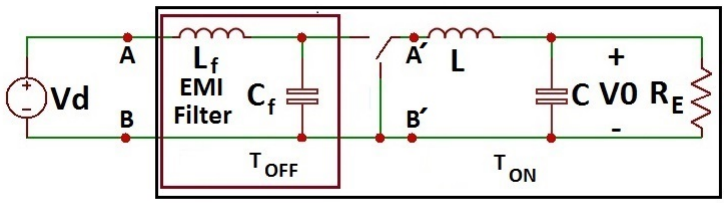


Figure 1. Buck converter.

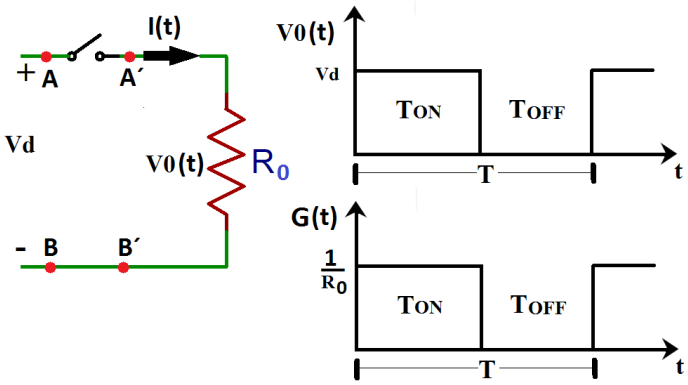


Figure 2. Switching circuit.

In order to model the nonlinear load, we propose a function $R(t)$ that replaces the nonlinear load at the A and B terminals, resulting in the simple configuration shown in Figure 3. In other words, this model represents the equivalent circuit after the storage sector, which could be seen as the nonlinear load $R(t)$. Notice that the switching effect of the transistor is included.

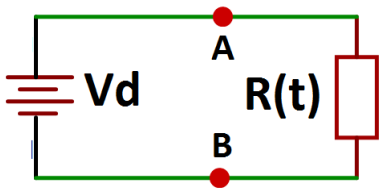


Figure 3. Nonlinear load $R(t)$ incorporated into the DCHN.

The voltage obtained at the A' and B' nodes of Figure 2, due to the effect of the transistor over the supply V_0, is given by the function:

$$V_0(t) = \begin{cases} V_d, & 0 \leq t \leq T_{ON} \\ 0, & T_{ON} \leq t \leq T_{OFF}, \end{cases} \tag{1}$$

where V_d is the voltage of the battery. Another important aspect to be considered is the current $I(t)$. According to Ohm's law, $I(t)$ is obtained as:

$$I(t) = \begin{cases} \frac{V_d}{R_0}, & 0 \leq t \leq T_{ON} \\ 0, & T_{ON} \leq t \leq T_{OFF}, \end{cases} \tag{2}$$

where R_0 denotes the resistance of the load. Since the voltage in the Equation (1), as a function of the time t, is periodical, it is possible to expand it in Fourier series

$$V_0(t) = \frac{a_0}{2} + \sum_{h=1}^{\infty} [a_h \cos(\frac{2h\pi t}{T}) + b_h \sin(\frac{2h\pi t}{T})], \tag{3}$$

where T is the switching period, and the various coefficients in the series are obtained in the usual way. In a similar manner, the current $I(t)$ in the Equation (2) can also be expanded as a Fourier series.

Let us consider Figure 2 again. The voltage between the nodes A and B is $V_d = Cte$. However, due to the switching effect of the transistor and R_0 between these nodes, there is an equivalent, time-dependent, resistance that can be described as:

$$R(t) = \begin{cases} R_0, & \text{if } 0 \leq t \leq T_{ON}, \\ \infty, & \text{if } T_{ON} \leq t \leq T_{OFF}. \end{cases} \tag{4}$$

Notice that the time interval $T_{ON} \leq t \leq T_{OFF}$ represents an open circuit state, while in the time interval $0 \leq t \leq T_{ON}$ the circuit is switched on and the current is still described by the Equation (2). Thus, the effect of the transistor plus R_0 is a simple equivalent circuit, shown in Figure 3, with $R(t)$ given in the Equation (4). This model represents the nonlinear load we referred to in the introduction.

On the other hand, instead of using $R(t)$, and to avoid dealing with the infinity resistance in the corresponding interval of time, we may use, equivalently, the reciprocal function, namely, the conductance $G_s(t)$ given by:

$$G_s(t) = \begin{cases} \frac{1}{R_0}, & \text{if } 0 \leq t \leq T_{ON} \\ 0, & \text{if } T_{ON} \leq t \leq T_{OFF}. \end{cases} \tag{5}$$

Since $G_s(t)$ is also a periodic function, it can be represented as a Fourier series. However, in order to circumvent cumbersome calculations involved in the Fourier expansion, we look for simplicity and propose a simple form describing the behavior of the conductance $G_s(t)$. We tested different functions to model the conductance and found that the periodic functions adjust well to the experimental behavior (and are given in the Equation (5)). An economical proposal to the function $G_s(t)$ is:

$$G(t) = G_h |\sin(\omega t)|^n = G_h |\sin(\pi f_s t)|^n, \tag{6}$$

where f_s is the switching frequency, G_h is the amplitude, n is the parameter to be determined, and $\omega = \frac{\omega_s}{2}$, being ω_s the angular switching frequency. Notice that as n increases, T_{ON} decreases in an inverse proportion. Actually, what we want to do is satisfy the fact that the area of the step function A_r be contained in the area A_c sustained by the function $G(t)$, shown in Figure 4. A basic condition for the Equation (6) is:

$$\int_{t=0}^{t=T} G(t)dt = \frac{T_{ON}}{R_0}, \tag{7}$$

that, for a n given, it gives the amplitude G_h. Equivalently, this relation can be expressed in terms of the time average:

$$\begin{aligned} < G(t) > &= \frac{1}{T_s} \int_0^{T_s} G(t)dt \\ &= \frac{D}{R_0}, \end{aligned} \tag{8}$$

where $D = T_{ON}/T$ is the duty cycle. Thus, from (8), we obtain:

$$G_h = \frac{\frac{n}{2}!^2 2^n D}{n! R_0}, \tag{9}$$

where we used G in Equation (6). Notice that Equation (8) defines the values of G_h. In order to get the value of the coefficient n, we used the Newton–Raphson method in the Equation (6). We obtain:

$$n = \frac{\tan((2-D)\frac{\pi}{4})}{\frac{D\pi}{4}}. \tag{10}$$

Notice that a cosine function can also be used; however, we prefer the sine function because it gives the proper initial conditions. In the next section we implement (6) in a practical circuit, subject to different conditions.

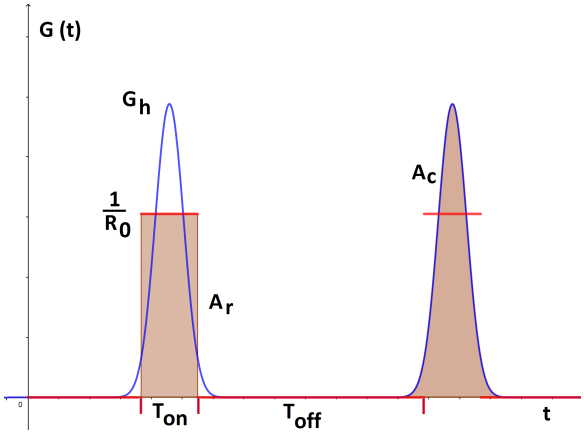
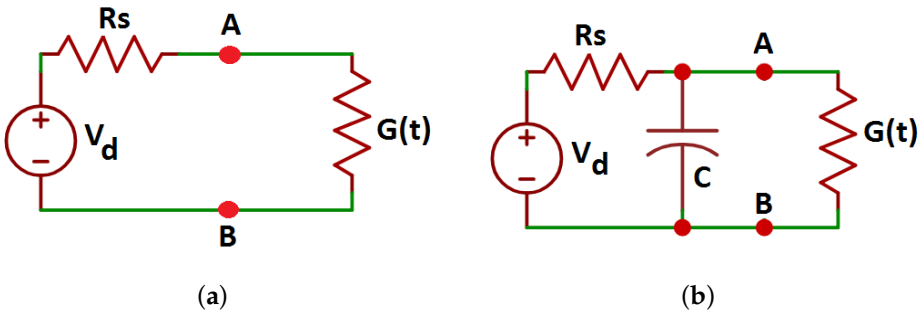


Figure 4. The duty cycle for the nonlinear load G(t).

The Model at Work

In order to obtain stability on microgrids, one looks for control of voltage and current to be as simple as possible in each DCHN [20,21]. However, due to the nonlinear behavior of the loads incorporated in the DCHN, the analysis of the electric parameters in the grid is difficult. There are several models in the literature that tackle this issue [22–24]. On the other hand, an SPS presents periodic behavior, in which the time T_{ON} corresponds to the maximal energy consumption, named the duty cycle D, while the time T_{OFF} occurs when the energy consumption is minimal, being $T_s = T_{ON} + T_{OFF}$ the period of the system. Thus, the switching frequency is $\omega_s = 2\pi/T_s$. Let us perform an analysis of the nonlinear loads by considering them as black boxes. The batteries set is represented with the supply V_d that feeds voltage to the DCHN. To find out the behavior of voltage and current in the presence of $G(t)$, we took the behavior of the battery V_d to be ideal. This allowed us to model an energy storage system in a simple manner. The resulting schematic circuit is a GC type, analogous to a RC circuit, shown in Figure 5a.



(**a**) (**b**)

Figure 5. Configuration. (**a**) Battery model. (**b**) EMI filter.

In this case, the resistance R_s models the internal resistance in the battery and other possible resistances, such as those resulting from the wiring. The battery feeds the circuit with a constant voltage V_d. The instantaneous current at the battery I_{Bat} can be calculated by Ohm's law as:

$$I_{Bat} = \frac{G(t)V_d}{G(t)R_s + 1}. \tag{11}$$

The voltage V_{AB}, between nodes A and B is given by:

$$V_{AB} = \frac{V_d}{G(t)R_s + 1}. \tag{12}$$

Thus, the instantaneous load power $P_G(t)$ is:

$$P_G(t) = V_{AB}(t)I_{Bat}(t) = \frac{G(t)V_d^2}{(G(t)R_s + 1)^2}. \tag{13}$$

Additionally, we can obtain the battery power $P_{Bat}(t)$:

$$P_{Bat}(t) = \frac{G(t)V_d^2}{G(t)R_s + 1}. \tag{14}$$

On the other hand, in order to reduce the voltage ripple in V_{AB}, it is common to use an EMI filter that can be composed of only one capacitor C. This allowed us to consider a circuit configuration, such as the shown in Figure 5b.

In this case, by applying Kirchhoff's laws to this circuit, the voltage in the capacitor is given by:

$$\frac{dV_c}{dt} + \frac{V_c(R_sG(t) + 1)}{R_sC} = \frac{V_d}{R_sC}, \tag{15}$$

which has an analytical solution as:

$$V_c(t) = e^{-\int \frac{R_sG(t)+1}{R_sC}dt}\left(\frac{V_d}{R_sC}\int e^{\int \frac{R_sG(t)+1}{R_sC}dt}dt + C_1\right), \tag{16}$$

where C_1 is the integration constant, which can be determined by giving the voltage at the initial time. For this configuration, the battery current results in:

$$I_{Bat}(t) = \frac{V_d - V_c(t)}{R_s}. \tag{17}$$

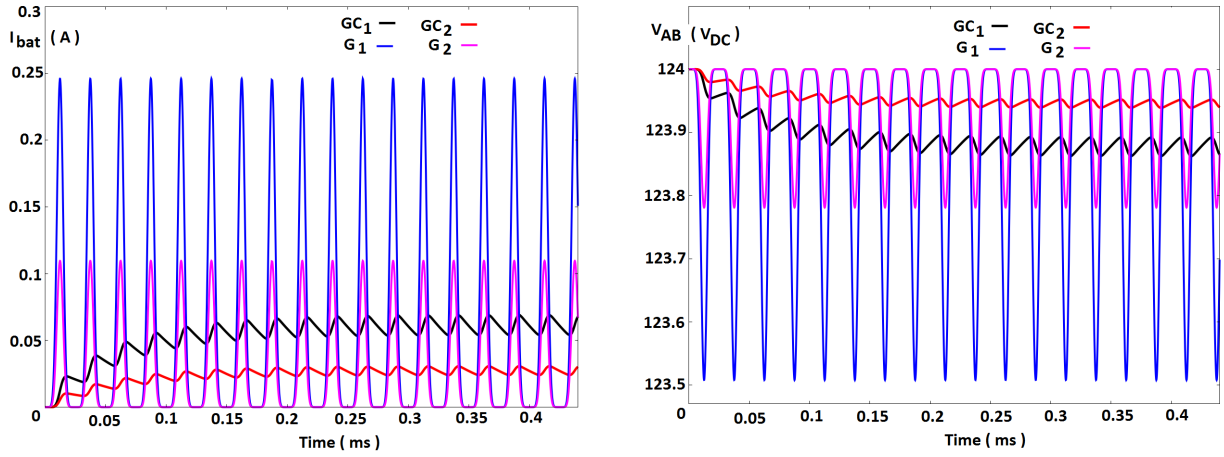
Additionally, the power supplied by the battery is given by:

$$P_{Bat}(t) = \frac{V_d^2}{R_s}\left(1 - \frac{V_c(t)}{V_d}\right). \tag{18}$$

In order to carry out numerical simulations, we used the Runge–Kutta fourth-order method and assessed the individual operation of the $G_1(t)$ and $G_2(t)$ loads with different values for the D, R_0, C and f_s parameters. We considered the initial condition for the voltage $V_c(0) = 124$V DC due to the nominal voltage of the our DCHN [25], and a value for R_s of 2 Ω. Both loads were incorporated in the circuits of Figure 5a,b, and their parameters are presented in Table 1. Finally, the numerical results for the voltage and current waveform are shown in Figures 6–9. In these figures, $GC_i, i = 1, 2$ stands for the presence of the capacitor C (EMI filter) and G_i without the capacitor in the circuit under analysis.

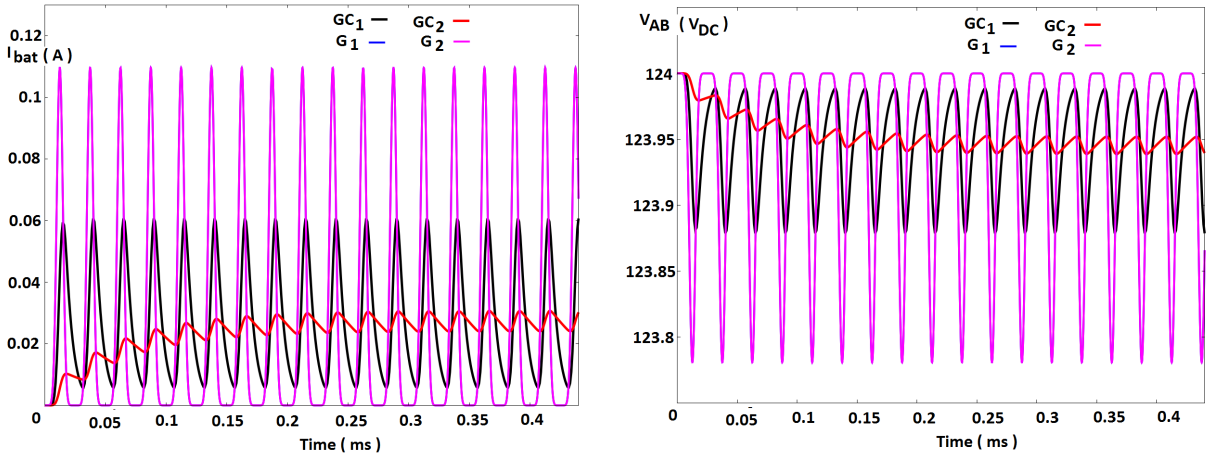
Table 1. Values of the parameters.

	Parameter	Case I	Case II	Case III	Case IV
$G_1(t)$					
	F_{s1}	40 KHz	40 KHz	40 KHz	40 KHz
	C_1	30 µF	3 µF	30 µF	30 µF
	D_1	0.4	0.4	0.32	0.4
	R_{O1}	8 Ω	18 Ω	18 Ω	18 Ω
$G_2(t)$					
	F_{s2}	40 KHz	40 KHz	40 KHz	38 KHz
	C_2	30 µF	30 µF	30 µF	30 µF
	D_2	0.4	0.4	0.4	0.4
	R_{O2}	18 Ω	18 Ω	18 Ω	18 Ω
	Current	Figure 6a	Figure 7a	Figure 8a	Figure 9a
	Voltage	Figure 6b	Figure 7b	Figure 8b	Figure 9b



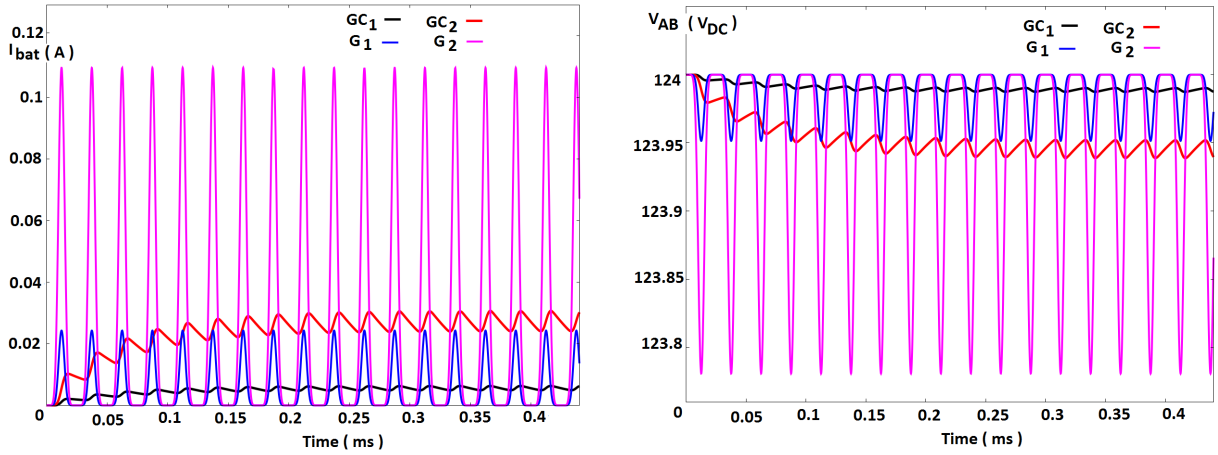
(**a**) (**b**)

Figure 6. Case I. (**a**) Battery current. (**b**) Voltage V_{AB}.



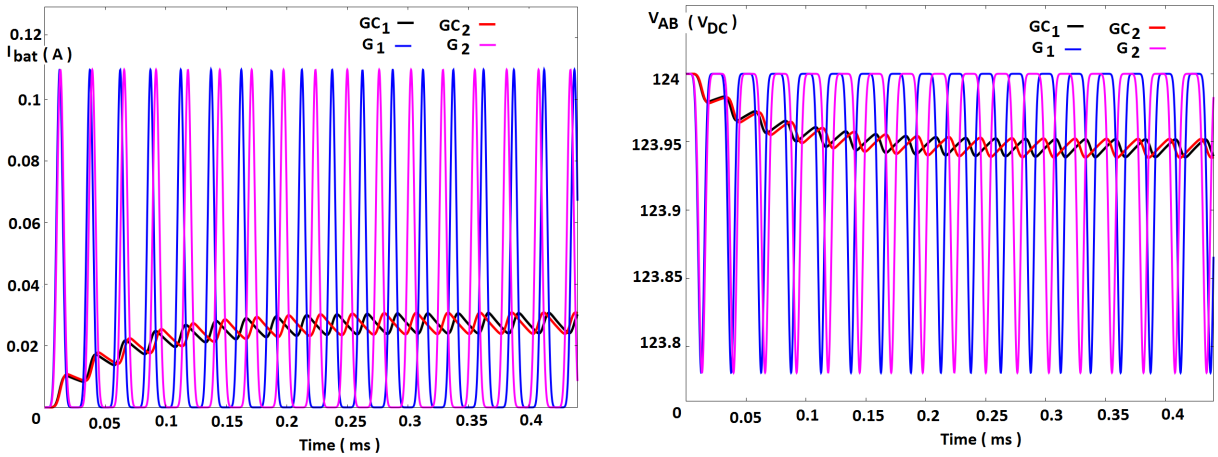
(**a**) (**b**)

Figure 7. Case II. (**a**) Battery current. (**b**) Voltage V_{AB}.



(**a**) (**b**)

Figure 8. Case III. (**a**) Battery current. (**b**) Voltage V_{AB}.



(**a**) (**b**)

Figure 9. Case IV. (**a**) Battery current. (**b**) Voltage V_{AB}.

3. Analysis of the Model

In a DCHN the simultaneous operation of two or more loads is common; for example, two or more LED lamps or a TV set and induction stove. However, the simultaneous operation of nonlinear loads in a DCHN leads to a more complex analysis, since previous knowledge of the internal components is necessary. In fact, each load is characterized by its own parameters of operation, such as the switching frequency, duty cycle, etc. We considered these parameters to carry out the analysis for two loads operating simultaneously. The features of each load can be different, such as in Figure 10. In this case, the energy store system fed the loads $R_1(t)$ and $R_2(t)$, the conductances of which were $G_1(t)$ and $G_2(t)$, respectively. In these resistances, there were currents $I_1(t)$ and $I_2(t)$. According to Kirchhoff's laws, we could read off the following equations:

$$V_d(t) - V_{R_s} = V_c(t) = V_1(t) = V_2(t), \quad (19)$$

$$I_{Bat}(t) = I_C + I_1 + I_2, \quad (20)$$

$$I_{G_{eq}}(t) = V_C(t)(G_1(t) + G_2(t)), \quad (21)$$

$$= V_C G_{eq}(t). \quad (22)$$

where we defined an equivalent conductance $G_{eq}(t)$ for this configuration as:

$$G_{eq}(t) = G_1(t) + G_2(t). \quad (23)$$

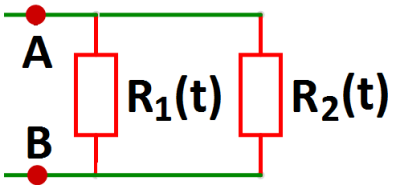


Figure 10. Two nonlinear loads R(t) operating simultaneously.

An illustration of this is shown in Figure 11. Let us mention that this model allows the possibility of a conductance with a dephasing ϕ, which, in practical results, is important. In the first place, we again considered G_{eq}, shown in Figure 10, for which we took the phase ϕ_1 for G_1, and ϕ_2 for G_2:

$$G_{eq_1}(t) = G_{h_1} \sin^{n_1}(f_{s_1}\pi t + \phi_1) + G_{h_2} \sin^{n_2}(f_{s_2}\pi t + \phi_2). \tag{24}$$

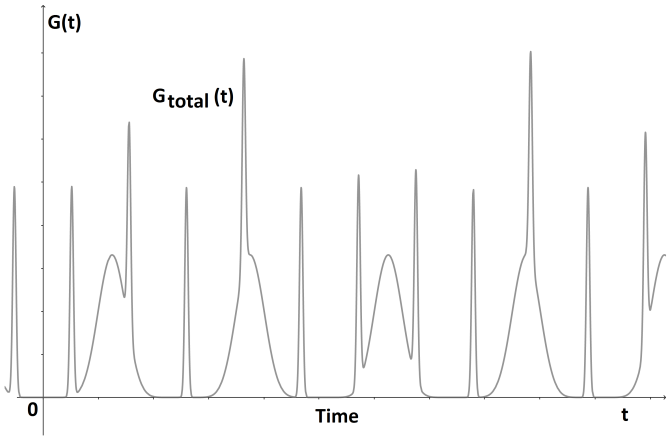
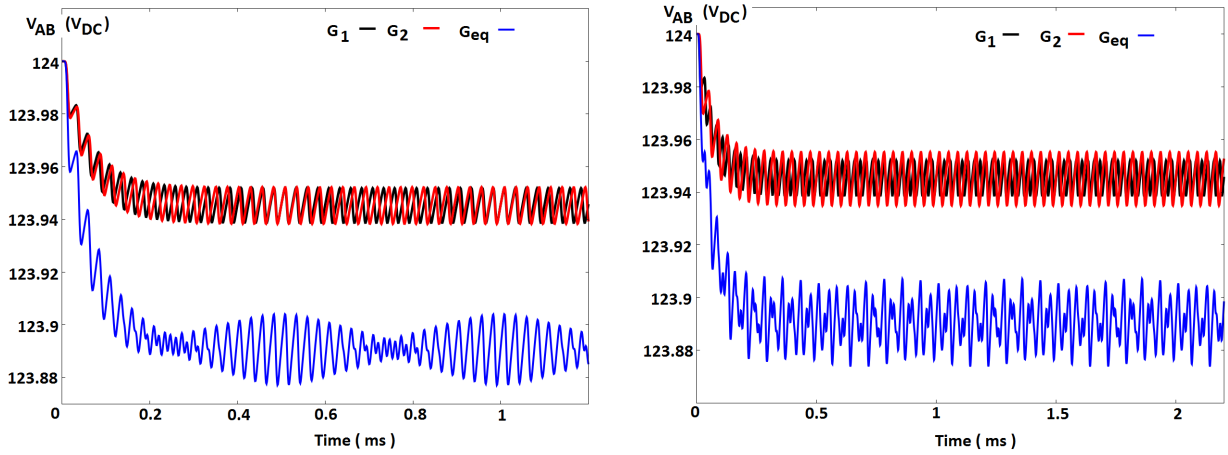


Figure 11. The equivalent conductance $G_{eq}(t)$.

Indeed, from (24) we obtained the numerical solution for the voltage in (15) by using the equivalent conductance. The simultaneous operation of the two loads with different frequencies is shown in Figure 12b. Let us consider the following parameters: load $G_1(t)$ having $f_{s_1} = 40$ KHz, $D_1 = 0.5$, $R_{0_1} = 430\ \Omega$, $\phi_1 = 0$, and for load $G_2(t)$: $f_{s_2} = 40$ KHz, $D_2 = 0.9$, $R_{0_2} = 3900\ \Omega$, and $\phi_2 = \frac{4\pi}{9}$. In Figure 13 the voltage for each of the loads and the voltage in G_{eq} are shown, considering individual and simultaneous operations, and for both cases we use $C = 30$ µF. In the next section, both the distortion waveform, when AC lighting devices are operating inside the DCHN, and the attenuation of the ripple, due the operation of the induction stove in stand by mode, are described.

As was mentioned, our model for nonlinear loads is so general that it could describe the nonlinear resistance behavior presented by any electric device that has an SPS as part of its design. Let us now present an analysis of our model applied to appliances in a DCHN, and compare the consequences with the respective results presented in the previous section. In order to describe the behavior of the SPS shown in Figure 2, we used the mathematical model in the Equation (6). The physical situation was characterized by a periodic conductance similar to the Equation (5), in which each of the periods intended to achieve an average conductance defined by the Equation (7). The former was used as an equivalent model of the circuit presented in Figure 3; the behavior of the conductance is shown in Figure 4.



(**a**) (**b**)

Figure 12. Simultaneous operation of the loads. (**a**) Voltage V_{AB}, for G_{eq}. (**b**) F_{s_1} = 40 KHz, F_{s_2}= 26 KHz.

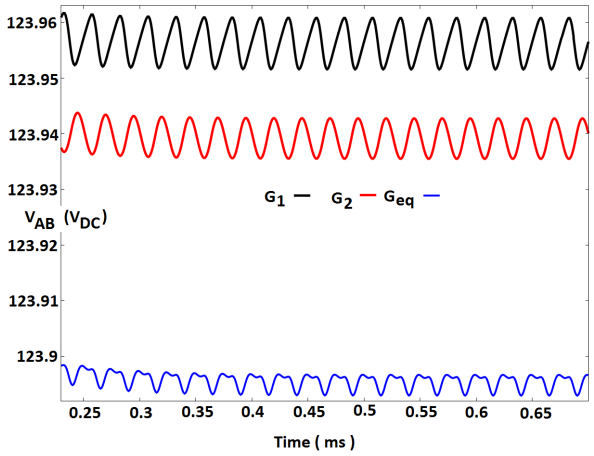


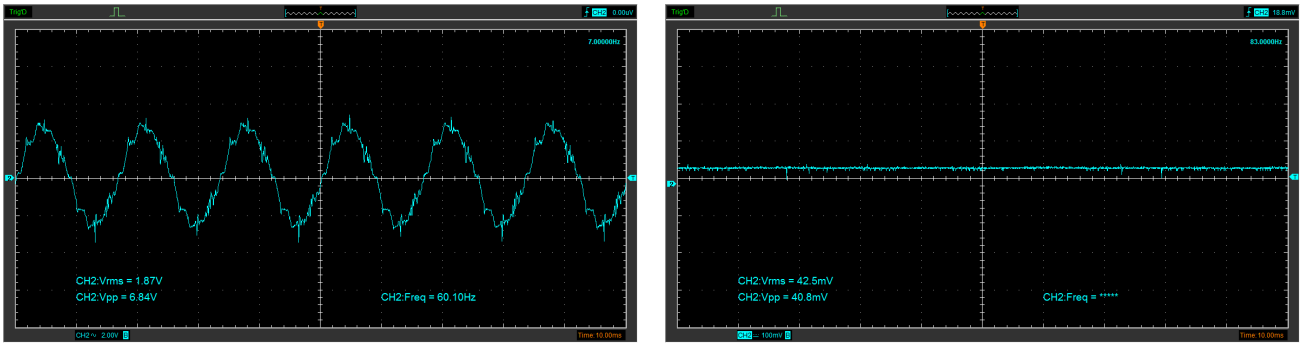
Figure 13. Voltage V_{AB} for a dephasing ϕ= $4\pi/9$ KHz.

The mathematical model was applied to different cases, as shown in Table 1. The various voltages and currents that were calculated are shown in Figures 6–9, and they correspond to individual operations of the $G_1(t)$ and $G_2(t)$ loads, with and without a capacitor. As can be appreciated in the aforementioned table, only a parameter was changed, keeping the rest of parameters fixed. In Case I, only the parameter R_0 varied, such that it took the values $R_{O1} = 8\ \Omega$ and $R_{O2} = 18\ \Omega$. For this case, the results for the current and voltage are shown in Figure 6a,b, respectively. According to the results, a higher energy consumption was observed in the load $G_1(t)$, and there was a larger voltage and current ripple. In Case II, C was varied, taking values $C_1 = 3\ \mu$F, and $C_2 = 30\ \mu$F. We observed that, when C increased, the voltage and current ripple diminished (see Figure 7a,b). In Case III, the duty cycle D changed, while the rest of the parameters were fixed. For this case, it was observed that the energy consumption increased as the duty cycle increased; hence, a higher voltage and current ripple were obtained, as shown in Figure 8a,b. Finally, Case IV corresponds to varying the switching frequency. The relation $F_{s2} < F_{s1}$ was used. For this case, the amplitude of the ripple of the voltage and current was equal in both loads, but with different frequencies (Figure 9a,b). Now, we considered the case of two loads operating simultaneously. The equivalent conductance behavior for both loads $G_1(t)$ and $G_2(t)$ is shown in Figure 11. Notice that (24) contained a constant phase in each of the loads. The voltage V_{AB}, due to the simultaneous operation of two loads, is presented in Figure 12a. The values of the parameters in Case IV of Table 1 were used in (23). As can be observed in Figure 12a a phenomenon of beats occurred. The simultaneous operation of

the loads could generate a ripple that resembled noise in the grid, even with the presence of an EMI filter, as can be observed in Figure 12b.

4. Experimental Study

In this section, the experimental results of current and voltage ripples are presented, as well as the standby consumption in a DCHN by an induction stove, and lighting lamps, respectively. For our analysis, we resorted to Ref. [26], which studied the possibility of incorporating AC lighting lamps into a DCHN, and analyzed the effects of CFL and LED lamps in a DC nanogrid. These lamps are associated with emission of harmonics in an AC grid [27]. The induction stove presents great consumption of energy in standby mode when it is connected to an AC grid, the current of which was measured as 1.87 A. The current waveform is shown in Figure 14a.



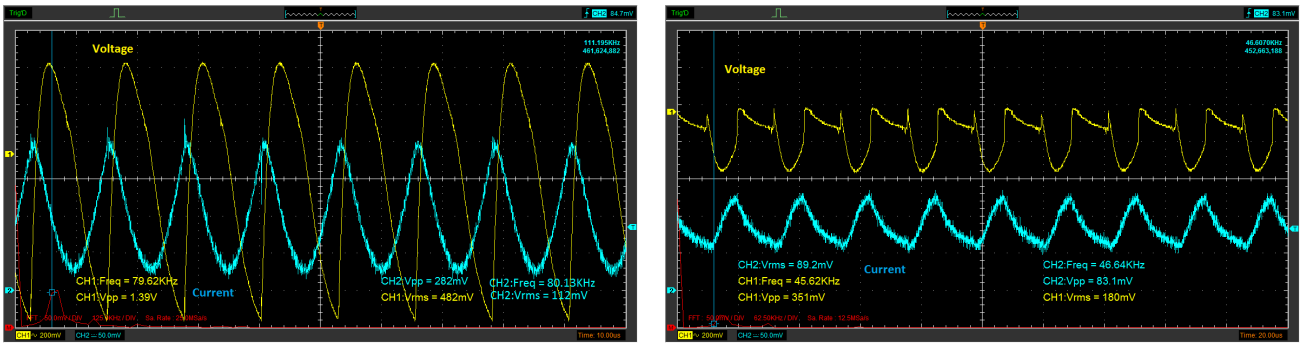
(**a**) (**b**)

Figure 14. The current waveform of the induction stove in standby mode. (**a**) At AC. (**b**) At DCHN.

Almost any induction stove could be incorporated directly into a DCHN without any modification. In fact, its internal voltage corresponds to DC, which is rectified by switching supplies from the AC grid.

We observed that the standby state consumption of the induction stove operating in the DCHN was very small and could be neglected. For this state, the current waveform is shown in Figure 14b, where the fundamental frequency corresponds to 0 Hz.

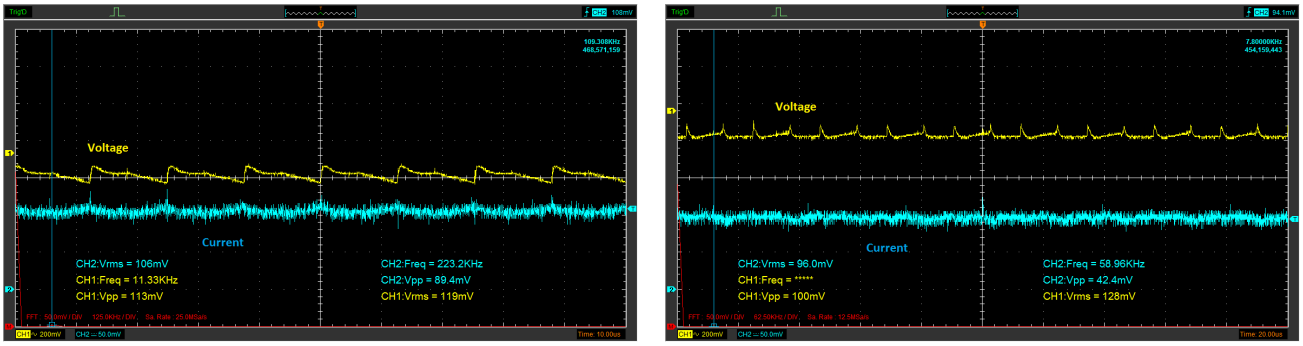
The graphs for the voltage and current ripple of the LED and CFL, when working in the DCHN, are shown in Figure 15a,b, respectively.



(**a**) (**b**)

Figure 15. The voltage and current ripple in the DCHN. (**a**) LED lamp. (**b**) CFL lamp.

It is usual for there to be simultaneous operation of two or more home appliances in a DCHN. In this case, we present the data of Figure 16a,b, obtained when the induction stove was in standby mode while the lighting devices were working. The experimental data in Table 2 correspond to the voltage and current ripple of the DCHN due to LED and CFL lamps.



(**a**) (**b**)

Figure 16. Attenuated voltage and current ripple in (**a**) LED lamp, and (**b**) CFL lamp due to the EMI filter at induction stove.

Table 2. Experimental data.

Device	Current $P_k - P_k$	Voltage $P_k - P_k$
C = 0		
LED lamp	282 mA	1.39 V
CFL lamp	83.1 mA	351 mV
C= 40 µF		
LED lamp	89.4 mA	113 mV
CFL lamp	42.4 mA	100 mV

The second case presented in Table 2, for which $C = 40$ µF, was due to the stand by mode of the induction stove (which contained the capacitor C). Notice that the filter capacitor in the induction stove reduced the voltage and current ripple in the DCHN. The capacitor element is located at the right side of the node AB in the circuit in Figure 5b. This side already corresponds to the load sector.

The simultaneous operation of one lamp and the induction stove in standby mode on the DCHN was also measured. We observed an attenuation in the ripple amplitude, due the capacitor in the induction stove, as shown in Figure 16a,b. It is interesting to note that the standby consumption of the induction stove, working on an AC system, was 1.8 A, while if it worked on a DCHN, the consumption was only 42.5 mA.

For each lighting device, we obtained periodical behavior in voltage and current ripple. For the LED lamp, we obtained an average frequency of 80 KHz (see Figure 15a). From Figure 15b, it can be observed that the average frequency was 46 KHz in the CFL voltage and current ripples. For the induction stove in standby mode, we observed a reduction in the voltage and current ripple due to the presence of the CFL or the LED lamp. The CFL voltage ripple diminished by 72% from the initial mode without the induction stove. The diminished CFL current ripple was about 49% of the initial value. The greatest diminishing was in the LED voltage ripple, which diminished by 91.87%; its final current ripple reduced to 68.3% .

5. Discussion

Let us compare the results of the proposed models for the load $G(t)$ with the experimental results. The solution of the circuit in Figure 5b by means of Equation (15) was worked out for the case of high frequencies. This solution showed the existence of low voltage and current ripple for lower consumption due to the high capacitance, which could be appreciated in Case III of Table 1 and related to Figure 16a,b. Notice that the voltage waveform (in blue) of Figure 13 obtained by the model was similar to the corresponding experimental results for the CFL presented in Figure 15b.

On the other hand, it is possible to relate the experimental data to the parameters of the model. In fact, for the case of the circuit without a capacitor, the peak-to-peak voltage V_{pp} can be defined by Equation (12) as:

$$V_{pp} = V_d(1 - \frac{1}{G_h R_s + 1}), \tag{25}$$

whereas the peak-to-peak current I_{pp} is given by:

$$I_{pp} = \frac{G_h V_d}{G_h R_s + 1}, \tag{26}$$

from which we obtain the amplitude of the conductance G_h in terms of the V_{pp} and I_{pp}:

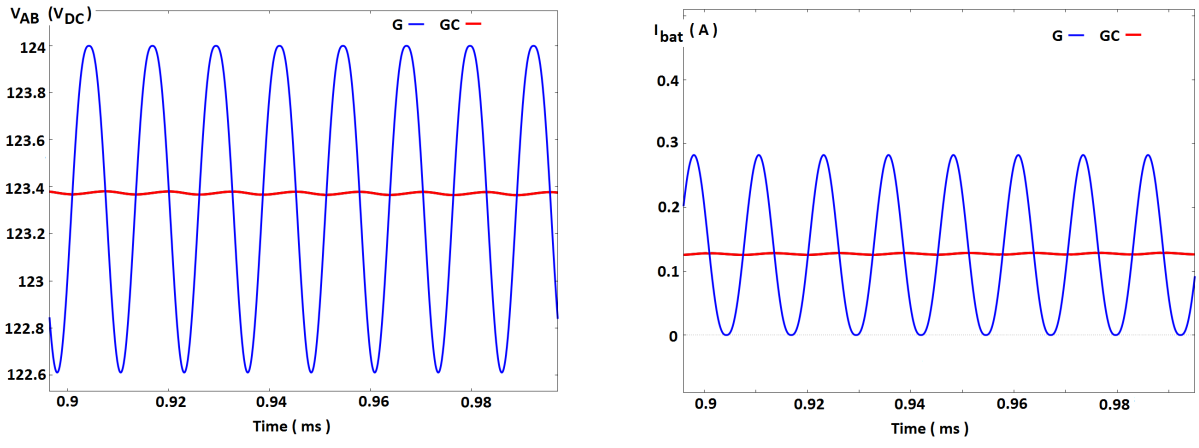
$$G_h = \frac{I_{pp}}{V_d - V_{pp}}. \tag{27}$$

This relation allows the model to reproduce the experimental data in an easy way. Furthermore, R_0 and R_s can be expressed in terms of V_{pp} and I_{pp}:

$$R_0 = \frac{(\frac{n}{2}!)^2 2^n D(V_d - Vpp)}{n! I_{pp}}, \tag{28}$$

$$R_s = \frac{V_{pp}}{I_{pp}}. \tag{29}$$

In order to test our model with the help of Equations (27) and (29), let us consider the experimental case of the LED lamp, shown in Figure 15a. The input data were $V_{pp} = 1.39$, $I_{pp} = 282$ mA. For the duty cycle, we took $D = 0.75$ for frequency $f_s = 79.62$ KHz, which were used in the Equation (15), along with the value of $C = 40$ µF. The results of the voltage and current ripple are shown in Figure 17a,b, respectively. The solution of the Equation (15) is given in the color red, while the initial voltage and current waveform correspond to color blue.

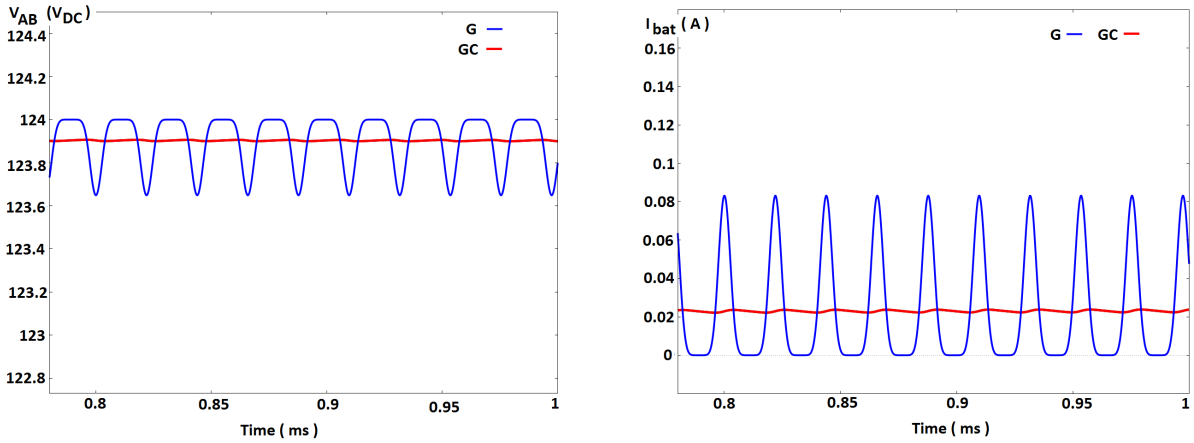


(**a**) (**b**)

Figure 17. Diminishing of the ripples due to the capacitor. (**a**) LED voltage ripple. (**b**) LED current ripple.

In the same way for the CFL from the Figure 15b, we used the following data: $f_s = 45.62$ KHz, $V_{pp} = 351$ mV, $I_{pp} = 83.1$ mA and $D = 0.45$. In Figure 18a,b the numerical solution of (15) for voltage and current waveform, respectively, are shown. Again, the red line corresponds to the solution with the capacitor and the solution without the capacitor is in blue. As far as the LED lamp and the CFL are concerned, the solution we obtained for these reproduced the initial profile of the voltage and current ripple, keeping the same amplitude, frequency and duty cycle. In Figure 19a,b we display the theoretical and experimental results for the voltage

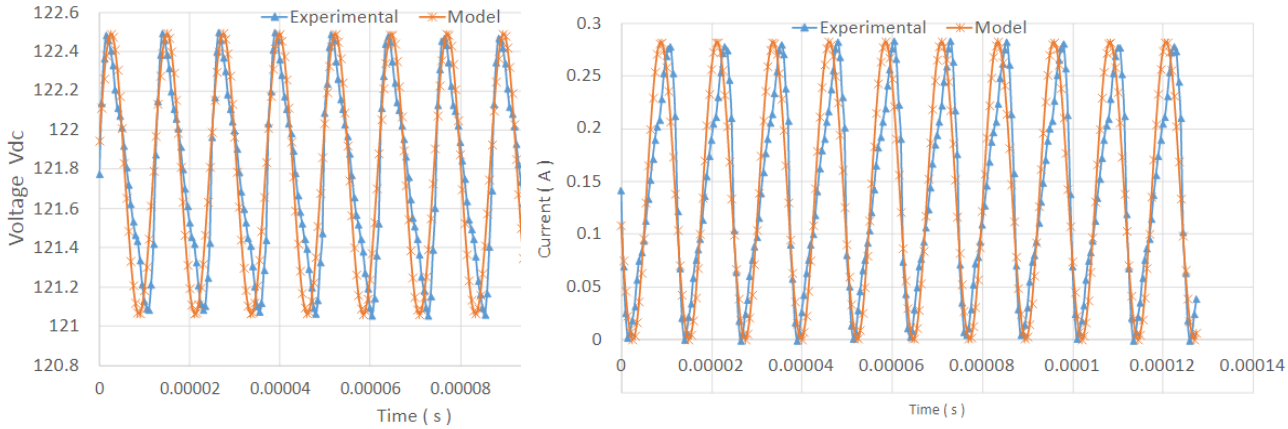
and current ripples due the LED lamp. As can be appreciated, there was great concordance between the experimental result and the result provided by the model.



(**a**) (**b**)

Figure 18. CFL model. (**a**) Voltage ripple. (**b**) Current ripple.

As can be observed, when the capacitor was used, the model predicted diminished voltage and current ripple.



(**a**) (**b**)

Figure 19. Experimental and theoretical data of the LED lamp. (**a**) Voltage waveform. (**b**) Current waveform.

Finally, it is interesting to note that the recovery effect in the voltage of the battery [28] was measured in the lamps of the DCHN, and shown in Figure 15a,b. The recovery effect emerged in our theoretical results due to the simple conditions for the storage energy model, since we defined it as an ideal battery which contains an internal resistance. It is also worth mentioning that this model, denoted as a function of the different parameters $G(V_{pp}, I_{pp}, D, f_s, t)$, does not require information on the features of the internal components of the devices. However, information such as V_{pp} and I_{pp} was necessary, which could be accessed from the experimental data.

6. Conclusions

In this work, we proposed a general model of nonlinear loads that describes the nonlinear resistance effect of electric devices due to the switching of the SPS inside devices such as home appliances used in a DCHN. By observing the periodic behavior of the load $R(t)$, we proposed the periodical behavior of the conductance $G(t)$. Our model can explain, numerically, the voltage ripple observed in an experimental setup. The model also allows the voltage ripple phenomenon in the DCHN with the simultaneous operation of

several home appliances to be understood. Other interesting features of the model are its simplicity in computational cost, since it is not necessary to have knowledge about the internal components in the appliances.

Home appliances incorporate an EMI filter into their components which attenuate noise interference in AC systems. Despite the fundamental frequency in the DCHN being zero, ripples with high frequencies are emitted into the DCHN, due the operation of lighting lamps. These high frequencies are equal to the switching frequencies of the SPS, and must be considered as interharmonics. With our model, we were able to explain the reduction of amplitude of the voltage ripple by increasing the capacitance in the circuit, which was corroborated by the experimental results. A higher capacitor value in the energy storage sector can improve the stability of the DCHN. However, the model is based on an equivalent circuit for a real nonlinear load, where the parameters G_h, and n must be adjusted by the values of D, R_0, and f_s used in each SPS. Through the model, we obtained a qualitative description of the voltage waveform corresponding to two different loads at the stationary state. With our model, along with (27) and (29), we were able to express the conductance in terms of V_{pp} and I_{pp}, which facilitated a comparison with the experimental results.

The localization of the capacitor in the load sector makes reducing the size of the energy storage sector possible. This makes the establishment of technical standards for the design and operation of the DCHN necessary, as well as an understanding of the behavior of these grids, in order to reach improved circuits to enlarge the life cycle in each DCHN sector. In such cases, the model could be useful for the issues aforementioned, since it explains the profiles of the ripples in voltage and current emitted into the DC nanogrid. However, the effects of ripples on different sectors of the DCHN remain unknown, but could be studied, under simple assumptions, by using the model.

Author Contributions: The authors contributed equally to the final dissemination of the research investigation as a full article. All authors have read and agreed to the published version of the manuscript.

Funding: The APC was funded by CIC-UMSNH.

Institutional Review Board Statement: Not applicable.

Informed Consent Statement: Not applicable.

Data Availability Statement: Not applicable.

Acknowledgments: The authors thank CONACYT, CIC-UMSNH and Tecnologico Nacional de Mexico for financial support.

Conflicts of Interest: The authors declare no conflict of interest.

Abbreviations

The following abbreviations are used in this manuscript:

DCHN	Direct Current Home Nanogrid
CFL	Compact Fluorescent Lamp
LED	Lighting Emission Diode
AC	Alternating Current
DC	Direct Current
SPS	Switching Power Supply
EMI	Electromagnetic Interference

References

1. Santoro, D.; Delmonte, N.; Simonazzi, M.; Toscani, A.; Rocchi, N.; Sozzi, G.; Cova, P.; Menozzi, R. Local Power Distribution A Review of Nanogrid Architectures, Control Strategies, and Converters. *Sustainability* **2023**, *15*, 2759. [CrossRef]
2. Munzke, N.; Schwarz, B.; Büchle, F.; Hiller, M. Evaluation of the efficiency and resulting electrical and economic losses of photovoltaic home storage systems. *J. Energy Storage* **2021**, *33*, 101724. [CrossRef]

3. Villanueva, D.; Cordeiro, M.; Feijóo, A.; Míguez, E.; Fernández, A. Effects of Adding Batteries in Household Installations: Savings, Efficiency and Emissions. *Appl. Sci.* **2020**, *10*, 5891. [CrossRef]
4. Sheridan, S.; Sunderland, K.; Courtney, J. Swarm electrification: A comprehensive literature review. *Renew. Sustain. Energy Rev.* **2023**, *175*, 113157. [CrossRef]
5. Lucía, Ó.; Cvetkovic, I.; Sarnago, H.; Boroyevich, D.; Mattavelli, P.; Lee, F.C. Design of home appliances for a DC-based nanogrid system: An induction range study case. *IEEE J. Emerg. Sel. Top. Power Electron.* **2013**, *1*, 315–326. [CrossRef]
6. Phannil, N.; Jettanasen, C.; Ngaopitakkul, A. Harmonics and Reduction of Energy Consumption in Lighting Systems by Using LED Lamps. *Energies* **2018**, *11*, 3169. [CrossRef]
7. Georgescu, G.; Neagu, B. The Pollution with Harmonics in Public Electric Energy Repartition and Distribution System. In Proceedings of the 3rd International Symposium on Electrical Engineering and Energy Converters, Suceava, Romania, 24–25 September 2009 ; pp. 251–256.
8. Rajput, S.K.; Dheer, D.K. Impact of Solar Intensity on Photovoltaic-Generated Current Harmonics and Transformer Life: A Mathematical Model With Experimental Validation. *J. Sol. Energy Eng.* **2023**, *145*, 021006. [CrossRef]
9. Chreang, S.; Kumhom, P. A study of nonlinear DC and AC loads connected to PV microgrid. In Proceedings of the 2018 5th International Conference on Business and Industrial Research (ICBIR), Bangkok, Thailand, 17–18 May 2018; pp. 309–313.
10. Venkatesh, C.; Kumar, D.S.; Sarma, D.S.; Sydulu, M. Modelling of nonlinear loads and estimation of harmonics in industrial distribution system. In Proceedings of the Fifteenth National Power Systems Conference (NPSC), IIT Bombay, Mumbai, India, 16–18 December 2008; pp. 592–597.
11. Caicedo, J.; Romero, A.; Zini, H. Frequency domain modeling of nonlinear loads, considering harmonic interaction. In Proceedings of the 2017 IEEE Workshop on Power Electronics and Power Quality Applications (PEPQA), Bogota, Colombia, 31 May–2 June 2017; pp. 1–6.
12. Rylander, M.; Grady, W.M. Problems in the use of Norton equivalent models for single-phase nonlinear loads. In Proceedings of the IEEE PES General Meeting, Minneapolis, MN, USA, 25–29 July 2010; pp. 1–7.
13. Nassif, A.B.; Yong, J.; Xu, W.; Chung, C. Indices for comparative assessment of the harmonic effect of different home appliances. *Int. Trans. Electr. Energy Syst.* **2013**, *23*, 638–654. [CrossRef]
14. George, V.; Bagaria, A.; Singh, P.; Pampattiwar, S.R.; Periwal, S. Comparison of CFL and LED lamp-harmonic disturbances, economics (cost and power quality) and maximum possible loading in a power system. In Proceedings of the 2011 International Conference & Utility Exhibition on Power and Energy Systems: Issues and Prospects for Asia (ICUE), Pattaya, Thailand, 28–30 September 2011; pp. 1–5.
15. Abdelkader, S.; Abdel-Rahman, M.; Osman, M. A Norton equivalent model for nonlinear loads. In Proceedings of the LESCOPE 01, 2001 Large Engineering Systems Conference on Power Engineering, Conference Proceedings, Theme: Powering Beyond 2001 (Cat. No. 01ex490), Halifax, NS, Canada, 11–13 July 2001; pp. 63–67.
16. Maher, M.; Abdel Aleem, S.H.; Ibrahim, A.M.; El-Shahat, A. Novel Mathematical Design of Triple-Tuned Filters for Harmonics Distortion Mitigation. *Energies* **2023**, *16*, 39. [CrossRef]
17. Wcislik, M.; Strzabala, P. Simulation Analysis of a Single-Phase AC Circuit with a Nonlinear Load. *Energies* **2023**, *16*, 1386. [CrossRef]
18. Fang, P.; White, B.; Fiorentino, C.; Liu, Y.F. Zero ripple single stage AC-DC LED driver with unity power factor. In Proceedings of the 2013 IEEE Energy Conversion Congress and Exposition, Denver, CO, USA, 15–19 September 2013; pp. 3452–3458.
19. Liao, J.; Zhou, N.; Wang, Q. Design of low-ripple and fast-response DC filters in DC distribution networks. *Energies* **2018**, *11*, 3128. [CrossRef]
20. Nasir, M.; Jin, Z.; Khan, H.A.; Zaffar, N.A.; Vasquez, J.C.; Guerrero, J.M. A Decentralized Control Architecture Applied to DC Nanogrid Clusters for Rural Electrification in Developing Regions. *IEEE Trans. Power Electron.* **2019**, *34*, 1773–1785. [CrossRef]
21. Mosayebi, M.; Sadeghzadeh, S.M.; Guerrero, J.M.; Khooban, M.H. Stabilization of DC Nanogrids Based on Non-Integer General Type-II Fuzzy System. *IEEE Trans. Circuits Syst. II Express Briefs* **2020**, *67*, 3108–3112. [CrossRef]
22. Francés, A.; Asensi, R.; García, O.; Prieto, R.; Uceda, J. A black-box modeling approach for DC nanogrids. In Proceedings of the 2016 IEEE Applied Power Electronics Conference and Exposition (APEC), Long Beach, CA, USA, 20–24 March 2016; pp. 1624–1631.
23. Arunkumar, G.; Elangovan, D.; Sanjeevikumar, P.; Nielsen, J.B.H.; Leonowicz, Z.; Joseph, P.K. DC grid for domestic electrification. *Energies* **2019**, *12*, 2157. [CrossRef]
24. Chekh, V.; Lyapunov, D.; Pravikova, A. Mathematical model of power supply system for remotely operated underwater vehicle with dc power transmission line and load voltage feedback. In *IOP Conference Series, Proceedings of the Materials Science and Engineering, Tomsk, Russia, 14–17 October 2019* ; IOP Publishing: Bristol, UK, 2021; Volume 1019, p. 012028.
25. Cordova-Fajardo, M.A.; Tututi, E.S. Incorporating home appliances into a DC home nanogrid. *J. Phys. Conf. Ser.* **2019**, *1221*, 012048. [CrossRef]
26. Cordova-Fajardo, M.A.; Tututi, E.S. How the Fluorescent and LED Lamps Affect the DC Home Nanogrids. In Proceedings of the 2020 IEEE Conference on Technologies for Sustainability (SusTech), Santa Ana, CA, USA, 23–25 April 2020; pp. 1–5.

27. Jiang, C.; Salles, D.; Xu, W.; Freitas, W. Assessing the collective harmonic impact of modern residential loads Part II: Applications. *IEEE Trans. Power Deliv.* **2012**, *27*, 1947–1955. [CrossRef]
28. Zhang, J.; Ci, S.; Sharif, H.; Alahmad, M. Modeling discharge behavior of multicell battery. *IEEE Trans. Energy Convers.* **2010**, *25*, 1133–1141. [CrossRef]

Disclaimer/Publisher's Note: The statements, opinions and data contained in all publications are solely those of the individual author(s) and contributor(s) and not of MDPI and/or the editor(s). MDPI and/or the editor(s) disclaim responsibility for any injury to people or property resulting from any ideas, methods, instructions or products referred to in the content.